

HOW COSMIC BACKGROUND CORRELATIONS AT LARGE ANGLES RELATE TO MASS AUTOCORRELATIONS IN SPACE

GEORGE R. BLUMENTHAL and KATHRYN V. JOHNSTON

UCO/Lick Observatory
Board of Studies in Astronomy and Astrophysics
University of California, Santa Cruz
Santa Cruz, California 95064

ABSTRACT

The Sachs-Wolfe effect is known to produce large angular scale fluctuations in the Cosmic Microwave Background Radiation (CMBR) due to gravitational potential fluctuations. We show how the angular correlation function of the CMBR can be expressed explicitly in terms of the mass autocorrelation function $\xi(r)$ in the Universe. We derive analytic expressions for the angular correlation function and its multipole moments in terms of integrals over $\xi(r)$ or its second moment, $J_3(r)$, which does not need to satisfy the sort of integral constraint that $\xi(r)$ must. We derive similar expressions for bulk flow velocity in terms of ξ and J_3 . One interesting result that emerges directly from this analysis is that, for angles θ , there is a substantial contribution to the correlation function from a wide range of distance r and that the radial shape of this contribution does not vary greatly with angle.

Subject Headings: Cosmic Microwave Background — Cosmology: Large Scale Structure of the Universe.

1 Introduction.

One sensible explanation for the currently clumpy state of the Universe is that it arose from the gravitational amplification of an initially nonuniform background mass density. The anisotropy of the Cosmic Microwave Background Radiation (CMBR) provides a signature of these primordial density perturbations. In simple terms, variations in the gravitational potential arising from density fluctuations at the last scattering surface produce variations in the redshift of photons across the sky. This is the Sachs-Wolfe effect (Sachs and Wolfe 1967, Wolfe 1968), which is the dominant contributor to CMBR fluctuations on large angular scales.

The CMBR anisotropy is most easily quantified in terms of the angular correlation function, $C(\theta) = \langle \delta T_1 \delta T_2 \rangle / \langle T \rangle^2$, of the temperature averaged over all directions in the sky; here θ is the angle between the directions 1 and 2. For potential fluctuations in a perturbed, flat, Friedmann universe, Sachs and Wolfe (1967) related $C(\theta)$ to the present power spectrum of matter fluctuations, $P(k)$, by following photon paths from the last scattering surface to the observer. Since the power spectrum itself is just given by the Fourier transform of the mass autocorrelation function $\xi(r)$, it is also possible to express $C(\theta)$ in terms of the autocorrelation function. This was done for some special cases by Traschen and Eardley (1986).

It is also well known that there are several other effects which can and do contribute to the CMBR anisotropy. These include Doppler shifts and thermalization effects associated with the surface of last scattering. However, on large angular scales, the dominant contributor to fluctuations is the Sachs-Wolfe effect.

In discussing the angular correlations of the CMBR, it is traditional to subtract out the contribution to $C(\theta)$ arising from its monopole and dipole moments (cf. Martinez-Gonzalez and Sanz 1989; Gorski 1991). The monopole term is not physically interesting, while the dipole contribution to the observed correlation of temperature is usually assumed to be dominated by the peculiar motion of the observer with respect to the local standard of rest. In that case the dipole velocity is not itself directly related to potential fluctuations. The recent positive detection by COBE of fluctuations in the CMBR (Smoot *et al.*, 1992) has been reported with monopole, dipole and quadrupole moments of $C(\theta)$ removed to exclude these large contributions to the anisotropy from sources other than the Sachs-Wolfe effect. For example, the Milky Way itself is a strong quadrupole source.

Another measure of large scale structure in the Universe which depends explicitly on the power spectrum $P(k)$ is the large scale bulk motion in the Universe (Lynden-Bell *et al.* 1988, Gorski 1991, Dekel *et al.* 1990).

A particularly useful quantity describing various models is the mean squared peculiar velocity $\langle v_p^2(R) \rangle$, averaged over some scale R .

In this paper, we derive explicit expressions for the peculiar velocity $\langle v_p^2(R) \rangle$ as well as the temperature correlation function $C(\theta)$, both with and without its first few moments removed, as integrals over the mass autocorrelation function, $\xi(r)$ or its own integral $J_3(r)$. We also derive similar expressions for each term in the multipole expansion of $C(\theta)$. In Section 2 we derive the basic relations, while in Section 3, we discuss how the various correlation functions interrelate.

2 Fundamental Relations

2.1 Definitions

In any N-dimensional space, the correlation function is a useful statistic of quantifying some of the relationships between values of a function at different spatial positions. The function can be continuous, as in the case of fluctuations in temperature or density, or it can even be discrete. A conceptually easy example of the latter is that of the autocovariance function of galaxies in three dimensions. Here it is a measure of the probability of finding a neighbor in the data set at a given distance from any galaxy (see Peebles, 1981, for example).

The correlation function of any continuous distribution is defined mathematically in terms of an average over all of N-dimensional space. Hence, the *angular correlation* of temperature fluctuations in the CMBR on the scale θ is defined as

$$C(\theta) = \frac{\langle \delta T_1 \delta T_2 \rangle}{\langle T \rangle^2}, \quad (1)$$

and the *mass autocorrelation* function for matter a distance r apart is given by

$$\xi(r) = \frac{\langle \delta \rho_1 \delta \rho_2 \rangle}{\langle \rho \rangle^2}. \quad (2)$$

The quantities δT and $\delta \rho$ are respectively the temperature and density excess over the mean, with subscripts 1 and 2 denoting position separated by an angle θ or distance r . The angular brackets signify averaging in two dimensions over the sky and over all three dimensional space. It is assumed that the correlations are independent of direction.

The *power spectrum* $P(k)$ is a measure of the amplitude of density perturbations in Fourier space for a given wave-number. It is defined simply as $|\delta_k|^2$, where δ_k is the Fourier transform of the dimensionless density excess $\delta \rho / \langle \rho \rangle$. As a result of these definitions, it is obvious that $P(k)$ is the three dimensional Fourier transform of $\xi(r)$. Since the autocorrelation function is independent of direction, one can write

$$P(k) = |\delta_k|^2 = 4\pi \int_0^\infty dr r^2 \xi(r) \frac{\sin kr}{kr}. \quad (3)$$

The power spectrum (3) often arises in expressions for observable quantities which arise from density or potential fluctuations. Any such observable quantity, Y , usually involves integrals in Fourier space of the form

$$Y(x) = \int_0^\infty dk k^2 P(k) F_Y(k, x). \quad (4)$$

The quantity $F_Y(k, x)$ explicitly relates the observed quantity Y (which may depend on some variable x) to the amplitude of waves having wavenumber k .

We can relate the observed quantity Y to the autocorrelation function by substituting for $P(k)$ from equation (3) and performing the k -integral to yield an expression involving an integral in real space. In this way we derive the *kernel*, $G_Y(r, x)$, for mass fluctuations, peculiar velocities and temperature variations in the CMBR, such that

$$Y(x) = \int_0^\infty dr r^2 \xi(r) G_Y(r, x). \quad (5)$$

This kernel is related directly to F_Y by the expression

$$G_Y(r, x) = \frac{4\pi}{r} \int_0^\infty dk k \sin(kr) F_Y(k, x), \quad (6)$$

or by the inverse expression

$$F_Y(k, x) = \frac{1}{2\pi^2 k} \int_0^\infty dr r \sin(kr) G_Y(r, x). \quad (7)$$

Integration by parts of equation (5) leads to

$$Y(x) = - \int_0^\infty dr J_3(r) \frac{\partial G_Y}{\partial r}, \quad (8)$$

where

$$J_3(r) = \int_0^r dr r^2 \xi(r). \quad (9)$$

Since by definition, $\xi(r)$ must satisfy the integral constraint $J_3(\infty) = 0$, while this is simply a boundary condition on J_3 , one can gain some insight into the underlying physics by considering (as in equation (8)) the derivative of the kernel $\partial G_Y/\partial r$ rather than the kernel G_Y itself.

2.2 Mass Fluctuations and Peculiar Velocities.

Consider a sphere having radius R . Then the mean squared mass excess in a randomly placed sphere of this radius is given by

$$\left\langle \left(\frac{\delta M}{M}(R) \right)^2 \right\rangle = \frac{1}{2\pi^2} \int_0^\infty dk k^2 P(k) W^2(kR), \quad (10)$$

where $W(kR)$ is the window function, which is given by a Fourier transform of a three dimensional top hat sphere of radius R :

$$W(kR) = \frac{3}{4\pi R^3} \int_{\text{sphere}} d^3\mathbf{r} e^{i\mathbf{k}\cdot\mathbf{r}} = \frac{3}{(kR)^3} [\sin kR - kR \cos kR] = 3 \frac{j_1(kR)}{kR}, \quad (11)$$

where j_1 is a spherical Bessel function. In analogy with eq. (5), we can rewrite equation (10) as

$$\left\langle \left(\frac{\delta M}{M}(R) \right)^2 \right\rangle = \int_0^\infty r^2 dr \xi(r) G_{\delta M}(r, R), \quad (12)$$

where equation (6) allows us to explicitly evaluate $G_{\delta M}$ as

$$G_{\delta M}(r, R) = \frac{3}{2R^3} \begin{cases} 2 - 3x + x^3, & \text{if } x < 1 \\ 0, & \text{otherwise,} \end{cases} \quad (13)$$

where $x = r/2R$. Clearly, $G_{\delta M}$ goes to zero for $r > 2R$ since correlations larger than the diameter of the sphere are irrelevant.

As an alternative to the top hat expression ((11)), one can smooth the power spectrum by weighting the points with a Gaussian window function of the form

$$W(kR_g) = e^{-k^2 R_g^2/2}, \quad (14)$$

where R_g is the Gaussian smoothing length. For this Gaussian window function, equation (6) allows us to obtain the kernel

$$G_{\delta M}(r, R) = \frac{1}{2\sqrt{\pi}R_g^3} e^{-r^2/4R_g^2}. \quad (15)$$

In a sense, (15) is obvious since it is again the window function in real space. Some papers relate the Gaussian smoothing length to the top hat sphere radius. For example, Blumenthal *et al.* (1992) require the Gaussian window to have the same spatial volume as the top hat sphere:

$$R_g = \left(\frac{2}{9\pi} \right)^{1/6} R, \quad (16)$$

while Lecar (1993) points out that for $R_g \approx .47R$, the Gaussian window function gives similar integrals to the top hat for a wide range of power spectra.

The kernels $G_{\delta M}$ for both the top hat window function and for the Gaussian window with R_g given by (16) are plotted in Figure 1a. Note that the expression for $\delta M/M$ follows directly from the definition of $\xi(r)$ rather than from an evolutionary calculation. Thus the kernel for the top-hat window is zero for distances larger than the distance across the top-hat ($2R$) since by definition, mass distributions are not sampled on these scales. The kernel for the Gaussian extends to cover all space since the weighted average is taken on all scales. In Figure 1b we have plotted the derivative of the kernel, which is used with the J_3 integral (8).

In a similar fashion, one can calculate, to first order in perturbation theory, the rms *peculiar velocity* averaged over randomly placed regions of size R :

$$\langle v_p^2(R) \rangle = \frac{H_o^2 \mathcal{F}^2(\Omega)}{2\pi^2} \int_0^\infty dk k^2 P(k) \frac{W^2(kR)}{k^2}, \quad (17)$$

where $\mathcal{F}(\Omega)$ is well approximated by $\Omega^{0.6}$ for density parameter $0 < \Omega < 1$ (Peebles 1976) and is approximately $\Omega^{4/7}$ for $\Omega \approx 1$ (Lightman and Schechter, 1991), and Ω is the dimensionless density parameter. Actually, \mathcal{F} represents the logarithmic rate of change of the amplitude of fluctuations with scale factor. The expression (17) is valid when the cosmological constant is zero, and \mathcal{F} must be modified in the case of a nonzero cosmological constant. H_o is the current value of Hubble's parameter. For a top-hat window, (6) yields the peculiar velocity kernel:

$$G_v(r, R) = \frac{H_o^2 \mathcal{F}^2(\Omega)}{R} \begin{cases} (\frac{6}{5} - 2x^2 + \frac{3}{2}x^3 - \frac{1}{5}x^5), & \text{if } x < 1 \\ \frac{1}{2x}, & \text{otherwise.} \end{cases} \quad (18)$$

The comparable expression using the Gaussian window-function (14) is given by

$$G_v(r, R) = \frac{H_o^2 \mathcal{F}^2(\Omega)}{r} \text{erf}(r/2R_g), \quad (19)$$

where erf is the error function.

The velocity kernels G_v (and their derivatives) for both the top-hat window and the Gaussian window with R_g given by (16) are also plotted in Figure 1. Here, the difference between top hat and Gaussian is more pronounced in the kernel derivative (Figure 1b) than in the kernel itself. This is a reflection of the fact that the autocorrelation function is in some sense a measure of the density distribution while J_3 measures the mass distribution and it is on this that the peculiar velocity is more heavily dependent. The kernel falls as r^{-1} on large scales ($r \gg R$). This behavior is obvious since the large scale contribution goes as $\langle v_p^2 \rangle \propto M(r)/r \propto \rho J_3(r)/r \propto \rho \xi(r)r^2 dr/r$, and large regions can have a significant effect on the velocity, as can be seen already from equation (17). It is also similar to the expression for mean squared velocity in Peebles 1981 (equation 14.10),

$$\langle v_p^2 \rangle = H_o^2 \mathcal{F}^2(\Omega) \int_0^\infty dr r \xi(r), \quad (20)$$

which explains the limiting behavior of $G_v \rightarrow H_o^2 \mathcal{F}^2(\Omega)/2Rx$.

Kashlinsky (1992) used a similar method to relate both the peculiar velocity correlation function ($\nu(r) = \langle \mathbf{v}_{p1} \cdot \mathbf{v}_{p2} \rangle$) to $\xi(r)$ and the rms peculiar velocity to the projected angular correlation function of matter, $w(\theta)$, found in the APM survey (Maddox *et al.*, 1990).

2.3 Angular Correlation Function.

The Sachs-Wolfe result for the CMBR angular correlation function is given by

$$\begin{aligned} C(\theta) &= \frac{H_o^4 \mathcal{F}(\Omega)}{8\pi^2 c^4} \int_0^\infty \frac{dk}{k^2} P(k) \frac{\sin ky}{ky} \\ &= \frac{H_o^4 \mathcal{F}(\Omega)}{c^4} \int_0^\infty dk k^2 P(k) F_C(k, \theta), \end{aligned} \quad (21)$$

where $y = 2R_h \sin(\theta/2)$ and $R_h = 2c/H_o\Omega$ (Sachs and Wolfe, 1967). Strictly speaking, this is the correct expression only for the Einstein-deSitter $\Omega = 1$, $\Lambda = 0$ universe, where Λ is the cosmological constant. When $\Lambda = 0$ and $\Omega \neq 1$, it is easy to generalize this for small enough angles corresponding to scales which crossed the horizon at early times when spatial curvature had little effect on the evolution of the Universe. Hence, for $\Omega < 1$, expression (21) is a good approximation for small angles $\theta < \Omega$ radians. In most cases, the Sachs-Wolfe effect is the dominant contributor to the background fluctuations for $\theta \gg 30'\Omega^{1/2}$; at these large angles, scattering effects are negligible.

A slight variant of equation (21) also remains a good approximation in the case of a zero curvature model with $\Lambda = 3(1 - \Omega)H_o^2/c^2$ (Kofman and Starobinsky 1985, Peebles 1984). Again, for small angles, Peebles (1984) showed that R_h should be replaced by the comoving distance

$$R_\Lambda = \frac{c}{H_o\Omega^{1/2}} \int_1^\infty dy (y^3 + \Omega^{-1} - 1)^{-1/2}, \quad (22)$$

and that the expression $\mathcal{F}(\Omega)$ should be replaced by an integral, which can be approximated as $\Omega^{1.54}$ (Efstathiou *et al.* 1992). So that our results can be valid for all these cases, we will investigate the kernel $F_C(k, \theta)$, defined in equation (21).

Expanding $F_C(k, \theta)$ in terms of Legendre polynomials shows the magnitude of the multipole contributions.

$$F_C(k, \theta) = k^{-4} \sum_{l=0}^{\infty} (2l+1) [j_l(kR_h)]^2 P_l(\cos \theta) = \sum_{l=0}^{\infty} f_l(k) P_l(\cos \theta), \quad (23)$$

where j_l are spherical bessel functions and P_l are Legendre polynomials. Figure 2 shows the amplitude of each of these contributions to the kernel (for fixed θ) as a function of wavenumber. The curves are each renormalized to a maximum of unity, and the monopole and dipole terms, which are singular at $k = 0$, are not shown. Clearly the dominant contribution to the integral in (21) for small k (corresponding to large spatial scales) is from the monopole and dipole moments as all others are finite at the origin. As Figure 2 shows, each subsequent, low order moment has a specific wavenumber associated with it, and picks out a small range of wavenumbers in the power spectrum $P(k)$. In particular, the quadrupole contribution is dominated by the very shortest wavenumbers. The position of the maximum is a monotonically increasing function of l , while the amplitude decreases with l . The distance in k -space between the maxima of adjacent l tends to a constant value while the width of the peak increases. Hence the strong association of a given wavenumber with a given term in the expansion weakens significantly for higher order terms.

In a similar fashion to equation (23), one can expand the spatial kernel in terms of Legendre polynomials:

$$G_C(\theta, r) = \sum_{l=0}^{\infty} g_l(r) P_l(\theta). \quad (24)$$

One normally ignores the monopole ($l = 0$) term since it represents only a renormalization of the mean temperature. Each of the $g_l(r)$ is related to the corresponding $f_l(k)$ from equation (23) using the integral (6). Defining $x = r/2R_h$, the dipole term is given by

$$g_1(r) = R_h \begin{cases} \frac{1}{10} - \frac{x^2}{6} + \frac{x^3}{8} - \frac{x^5}{60}, & \text{if } x < 1 \\ \frac{1}{24x}, & \text{otherwise.} \end{cases} \quad (25)$$

This term is normally ignored as well in cosmological comparisons since the major contributor to the observed dipole is thought to be the Doppler shift coming from the peculiar motion of our own galaxy. Doppler terms were explicitly excluded in Sachs and Wolfe's original calculation. The fact that contributions to the dipole can come from scales larger than the horizon lends credence to the argument (Paczynski and Piran, 1990) that it is possible for a significant part of the dipole moment not to be Doppler in origin.

The higher order moments are all zero for $x > 1$. For $x < 1$ and $l > 1$ we find the general result

$$g_l(r) = R_h \left[\frac{1}{2(2l+3)(2l-1)} - \frac{1}{6}x^2 + \frac{(2l+1)}{12} \sum_{k=0}^l \frac{(-1)^k (l+k)!}{(l-k)!(k!)^2} \left(\frac{2}{2k+1} - \frac{3}{1+k} + \frac{6}{2k+3} - \frac{1}{k+2} \right) x^{2k+3} \right]. \quad (26)$$

Figure 3a shows plots of these spatial kernels. The curves are again renormalized to a maximum of unity, and the monopole term, which is singular, is not plotted. All moments of higher order than the dipole are zero beyond the horizon and have $(l - 1)$ zero points within it. As in the equivalent k -space plot (figure 2) the maximum value decreases with increasing l . Here there is no specific distance associated with any given l as all the peaks are at the origin. However, there is some suggestion to a characteristic *range* in r for each l as the width of the peaks decreases monotonically.

Figure 3b plots the derivatives of the functions shown in figure 3a, which are relevant for the J_3 integration. Higher moments have maxima at progressively smaller scales, just as implied by the case in k space. Essentially, higher moments arise from correlations (or mass concentrations) at smaller spatial scales. Note that these curves have once again been renormalized and the amplitude of the initial peak actually decreases with l . Because correlations at a given angle θ involve sums over many values of l , these plots (figures 3a and b) lead us to expect that such correlations do not arise from fluctuations on a specific associated spatial scale, but rather from similar ranges in r .

One can also transform the general kernel, $F_C(\theta, k)$ defined in equation (23). Defining $s \equiv \sin \theta/2$, the kernel for the correlation function with the monopole term removed (to get rid of singularities) is

$$G_C(\theta, r) = R_h \begin{cases} \left(\frac{1}{6} - \frac{s}{4}\right) + \left(\frac{1}{6} - \frac{1}{12s}\right)x^2 - \frac{x^3}{24}, & \text{if } 0 < x < s \\ -\frac{s^2}{12x} + \frac{1}{6} - \frac{x}{4} + \frac{x^2}{6} - \frac{x^3}{24}, & \text{if } s < x < 1 \\ (1 - 2s^2)\frac{1}{24x}, & \text{otherwise.} \end{cases} \quad (27)$$

This agrees with a transform of the function derived from first principles by Traschen and Eardley (1986). The derivative function is given by

$$\frac{\partial}{\partial r} G_C(\theta, r) = \begin{cases} \left(\frac{1}{6} - \frac{1}{12s}\right)x - \frac{x^2}{16}, & \text{if } 0 < x < s \\ \frac{s^2}{24x^2} - \frac{1}{8} + \frac{x}{6} - \frac{x^2}{16}, & \text{if } s < x < 1 \\ -(1 - 2s^2)\frac{1}{48x^2}, & \text{otherwise.} \end{cases} \quad (28)$$

Contour plots of $G_C(\theta, r)$ and its derivative are shown in Figures 4a and 4b respectively, with the dipole term also removed. These figures demonstrate that there is very little tendency for correlations at a given angle to correspond to a given spatial distance r for either the integral involving $\xi(r)$ or the one involving $J_3(r)$. Such a tendency may exist for very small angles of a few degrees or less, but for the most part, it is absent.

This is further demonstrated in Figures 5 and 6. In Figures 5a and 5b we show slices through the contour maps in Figures 4a and 4b. Essentially all of the curves (for all angles shown) give significant contributions to $C(\theta)$ from similar regions of space. Figures 6a and 6b present similar results but with the quadrupole term removed as well. Now the curves have more structure, but there is again little or no tendency for correlations on larger angles to arise from greater distances.

3 Conclusions.

We have derived explicit relations between the mass autocorrelation function $\xi(r)$ and the angular correlation of background radiation on the sky $C(\theta)$ due to the Sachs-Wolfe effect. We also derived expressions relating $C(\theta)$ (as well as its multipole moments) to the second moment of $\xi(r)$, namely $J_3(r)$. We argued that the integral involving $J_3(r)$ is in some sense the more fundamental, since unlike the autocorrelation function, $J_3(r)$ does not satisfy an integral constraint. Because of the integral constraint, the kernel $G_C(\theta, r)$ does not provide the unique contribution from every radius r since every positive correlation must be balanced by a negative correlation somewhere else. $J_3(r)$ does not suffer this problem.

The expressions derived here may be used either with theoretical or observed mass autocorrelation functions to derive the microwave background fluctuations. Of course, it is true that large galaxy surveys can be used to derive either an autocorrelation function or a power spectrum (Davis and Peebles 1983, Maddox *et al.*, 1990). Hence either equation (21) or equation (27) can in principle be used to derive the anisotropy. However, the spatial integral provides a direct measure of the volume that must be surveyed to obtain an accurate result at a given angle. If the dipole term (equation (25)) is also removed from the kernel it does not require integration over scales larger than the horizon.

The most surprising result that we find is that mass fluctuations on all spatial scales contribute to temperature fluctuations on any but the very smallest angular scales, as is demonstrated in Figures 4 and 5. This arises in part because the correlation at any angle is the sum of contributions from many multipole moments. Although there is a clear tendency for the higher multipole moments to arise from smaller distances r , when one adds the many multipole moments to obtain G_C , this tendency disappears. Hence it is dangerous and incorrect to assume that each angle θ is related to a unique distance scale r for any correlation.

We would like to thank Luiz DaCosta and Sandra Faber for helpful discussions. This work was supported in part by grants from NSF, NASA, and a UCSC faculty research grant.

Figure Captions

- Figure 1 a.** Derived kernels for mass fluctuations and bulk velocities. $R^3 G_{\delta M}$ plotted for a top-hat window function of radius R (solid line) and a Gaussian window of the same volume (dotted line). $R G_v / H_0^2 \mathcal{F}^2(\Omega)$ plotted for a top-hat window (short dashed line) and a Gaussian window (long dashed line). **b.** Kernels for integration over J_3 found by differentiating the functions shown in Figure 1a.
- Figure 2** Amplitude of multipoles of the k -space kernel $f_l(k)$ for $l = 2, 3, \dots, 6$. These curves have been renormalized to a maximum of unity.
- Figure 3 a.** Amplitude of multipoles for the real-space kernel, $g_l(r)$ for $l = 1, 2, \dots, 6$. The curves have been renormalized to give a maximum of unity. **b.** Kernels for integration over J_3 found by differentiating the functions shown in Figure 3a. The curves have been renormalized to give a maximum of unity.
- Figure 4 a.** Contours of $G_C(r, \theta) / R_h^3$ with monopole and dipole only subtracted. The maximum occurs at $\theta = r = 0$ and has value $\frac{1}{15}$. Negative contours are indicated by dashed lines. Levels are shown at logarithmic intervals with spacing of $.4dex$ with the zero level contour in bold and the lowest magnitude contour at 10^{-6} . **b.** Derivatives of function shown in Figure 4a.
- Figure 5 a.** The value of the kernel $G_C(\theta, r) / R_h^3$ (with the monopole and dipole removed) for $s = \sin(\theta/2) = 0.1, 0.3, 0.5, 0.7, 0.9$ as functions of r . These are just slices through Figure 4a. **b.** Kernels for integration over J_3 found by differentiating the functions shown in Figure 5a.
- Figure 6 a.** The value of the kernel $G_C(\theta, r) / R_h^3$ (with the monopole, dipole, and quadrupole removed) for $s = \sin(\theta/2) = 0.1, 0.3, 0.5, 0.7, 0.9$ as functions of r . This is the same as Figure 5a but with the quadrupole removed as well. **b.** Kernels for integration over J_3 found by differentiating the functions shown in Figure 6a.

References.

- Blumenthal, G. R., da Costa, L. N., Goldwirth, D. S., Lecar, M. and Piran, T. 1992 *Ap. J.* 388, 234.
- Davis, M. and Peebles, P.J.E. 1983 *Ap. J.* 267, 465.
- Dekel, A., Bertschinger, E., and Faber, S.M., 1990, *Ap. J.* 364,349.
- Efstathiou, G., Bond, J. R. and White, S. D. M. *M.N.R.A.S.* 258, 1P.
- Gorski, K. 1991), *Ap. J. Lett.* 370, L5.
- Kashlinsky, A. 1992, *Ap. J.* 386, L37.
- Kofman, L. A. and Starobinsky, A. A. 1985, *Soviet Astr. Lett.* 11, 271.
- Lightman, A.P. and Schechter, P.L., 1990, *Ap. J. Suppl.* 74,831.
- Lecar, M. 1993, Private Communication.
- Lynden-Bell, D., Faber, S.M., Burstein, D., Davies, R.L., Dressler, A., Terlevich, R.L. and Wegner, G., 1988, *Ap. J.* 326,19.
- Maddox, S.J., Efstathiou, G., Sutherland, W. J. and Loveday, J., 1990, *M.N.R.A.S.* 242 43P.
- Martinez-Gonzalez, E., and Sanz, J. L. 1989, *Ap. J.* 347,11.
- Paczynski, B., and Piran, T., 1990, *Ap. J.* 364, 341.
- Peebles, P. J. 1976, *Ap. J.* 205, 318.
- Peebles, P. J. E. 1981 *Large Scale Structure in the Universe.* (Princeton University Press).
- Peebles, P. J. E. 1984, *Ap. J.* 284, 439.
- Sachs, R. K. and Wolfe, A. M. 1967, *Ap. J.* 147,73.
- Smoot, G. F., Bennet, C. L., Kogut, A., Wright, E. L., Aymon, J., Boggess, N.W., Cheng, E.S., De Amici, G., Gulkis, S., Hauser, M.G., Hinshaw, G., Lineweaver, C., Loewenstein, K., Jackson, P. D., Janssen, M., Kaita, E., Kelsall, T., Keegstra, P., Mather, J., Meyer, S. S., Moseley, S. H., Murdock, Y., Rokke, L., Silverbeg, R. F., Tenorio, L., Weiss, R. and Wilkinson, D. T. 1992, *Ap.J.* 388, 234.
- Suto, Y., Gorski, K., Juskiewicz, R. and Silk, J. 1988, *Nature* 332, 328.
- Traschen, J. and Eardley, D. M. 1986, *Phys. Rev. D* 34, 6.
- Wolfe, A.M., 1968, *Ap.J.* 156, 803.

This figure "fig1-1.png" is available in "png" format from:

<http://arxiv.org/ps/astro-ph/9402032v1>

FIGURE 1a

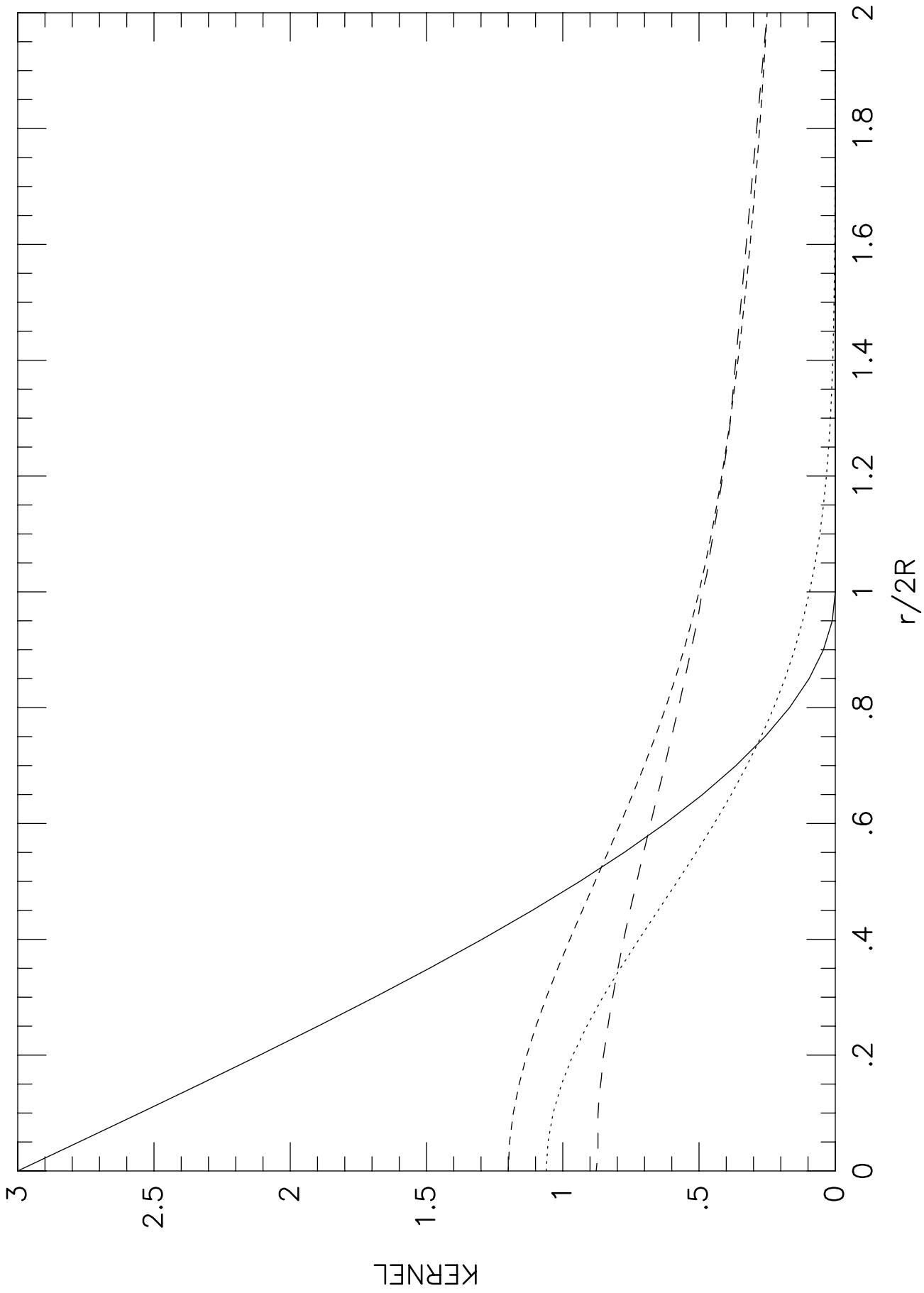
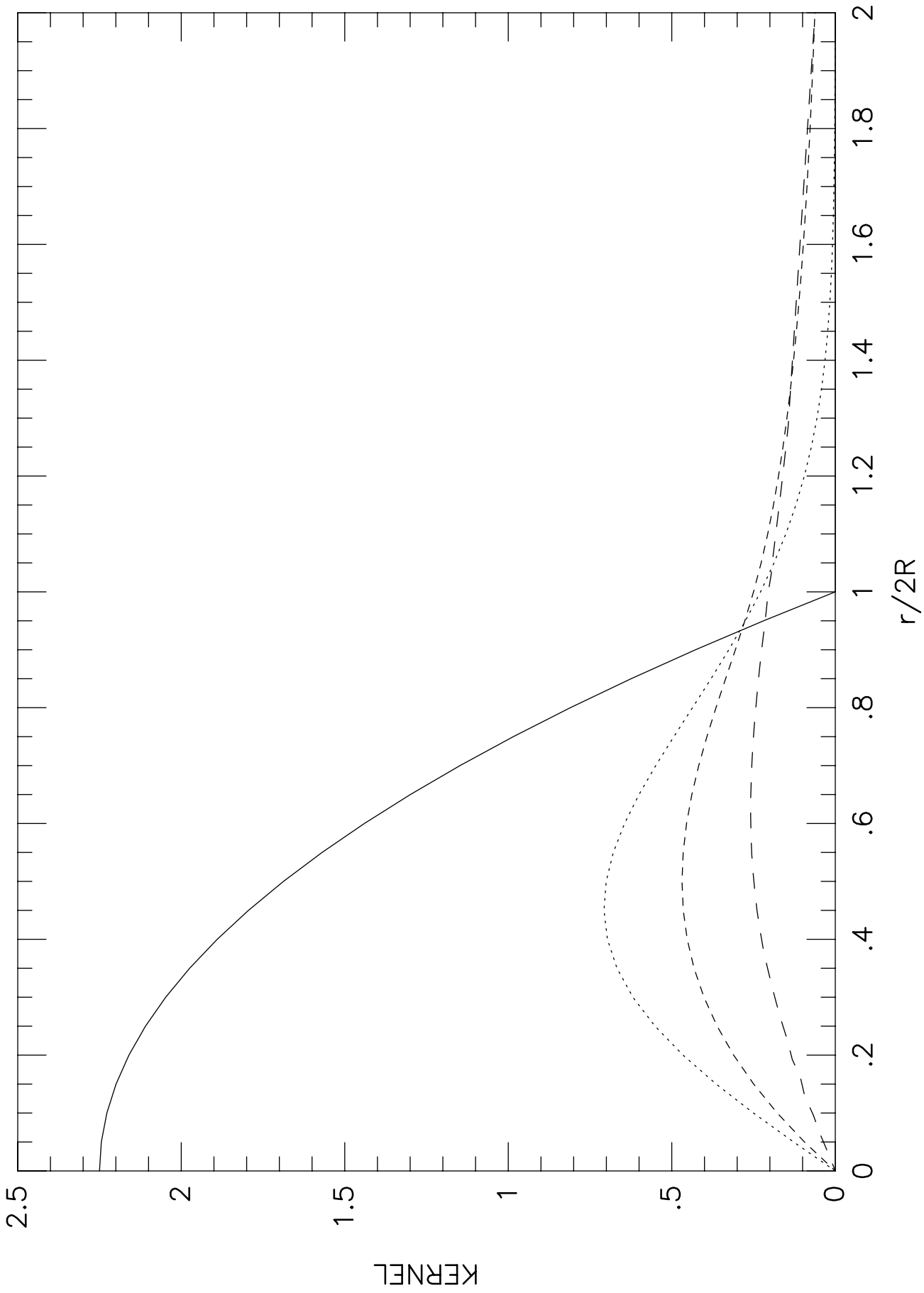


FIGURE 1b



This figure "fig2-1.png" is available in "png" format from:

<http://arxiv.org/ps/astro-ph/9402032v1>

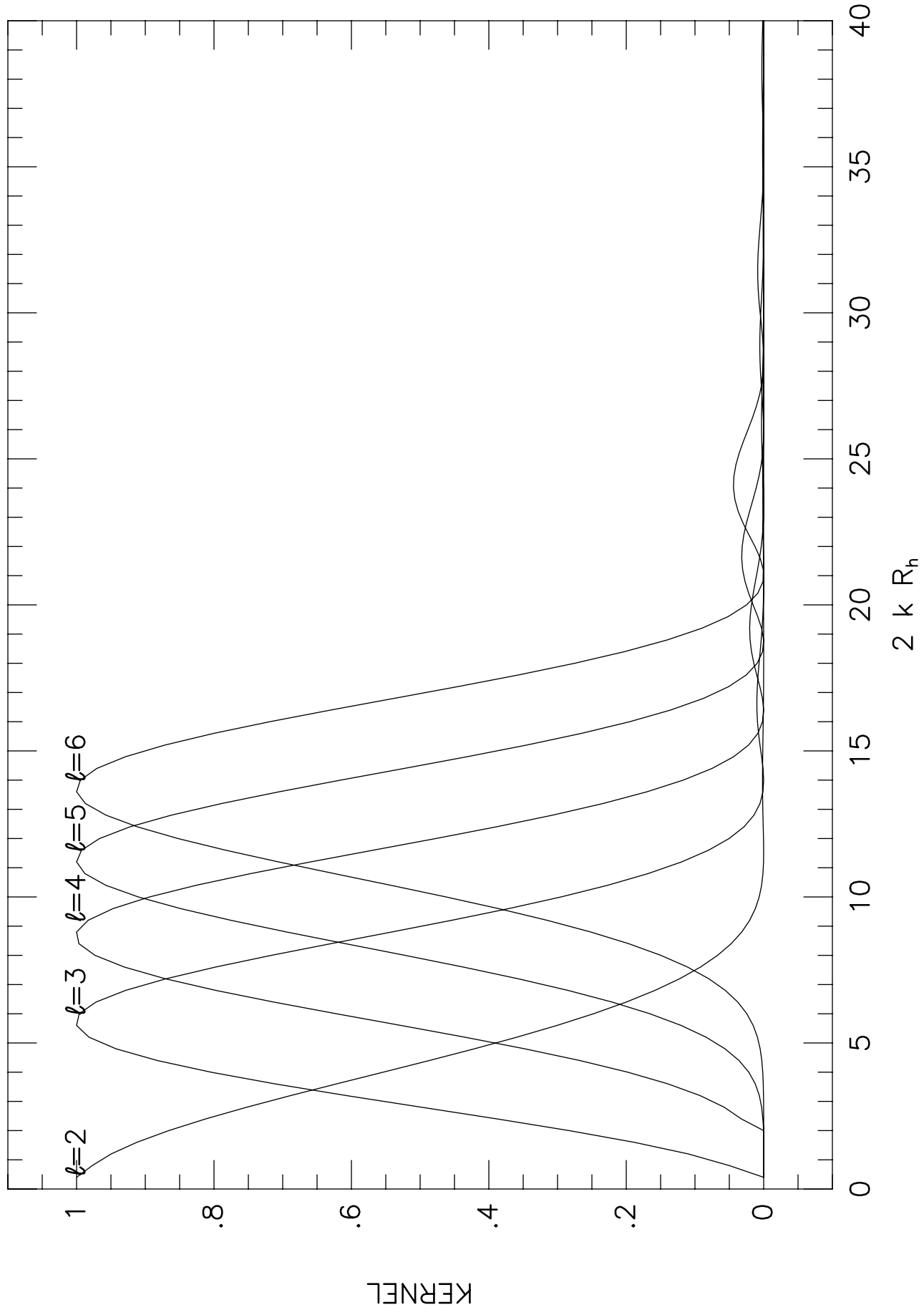
This figure "fig1-2.png" is available in "png" format from:

<http://arxiv.org/ps/astro-ph/9402032v1>

This figure "fig2-2.png" is available in "png" format from:

<http://arxiv.org/ps/astro-ph/9402032v1>

FIGURE 2



This figure "fig1-3.png" is available in "png" format from:

<http://arxiv.org/ps/astro-ph/9402032v1>

This figure "fig2-3.png" is available in "png" format from:

<http://arxiv.org/ps/astro-ph/9402032v1>

FIGURE 3a

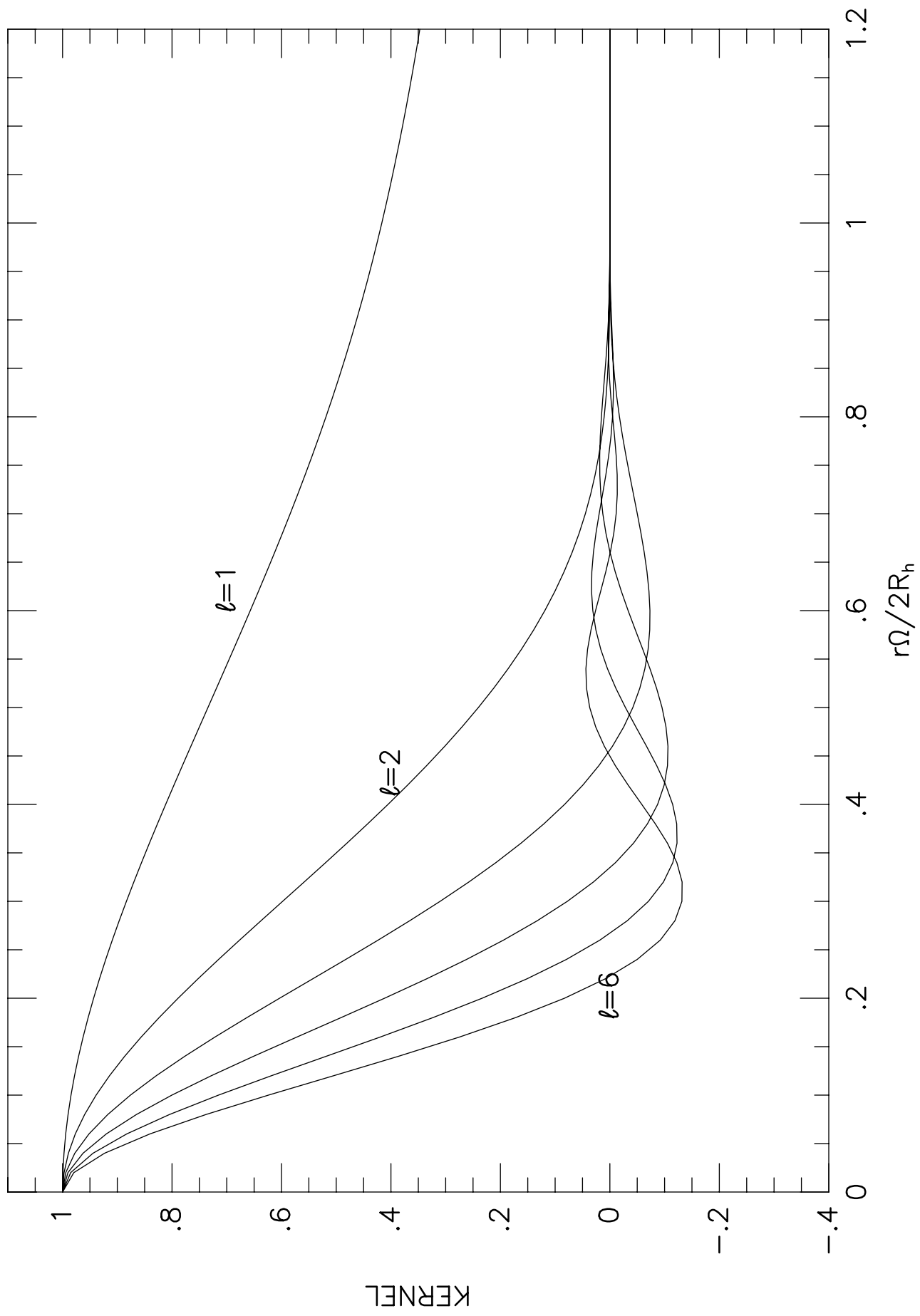
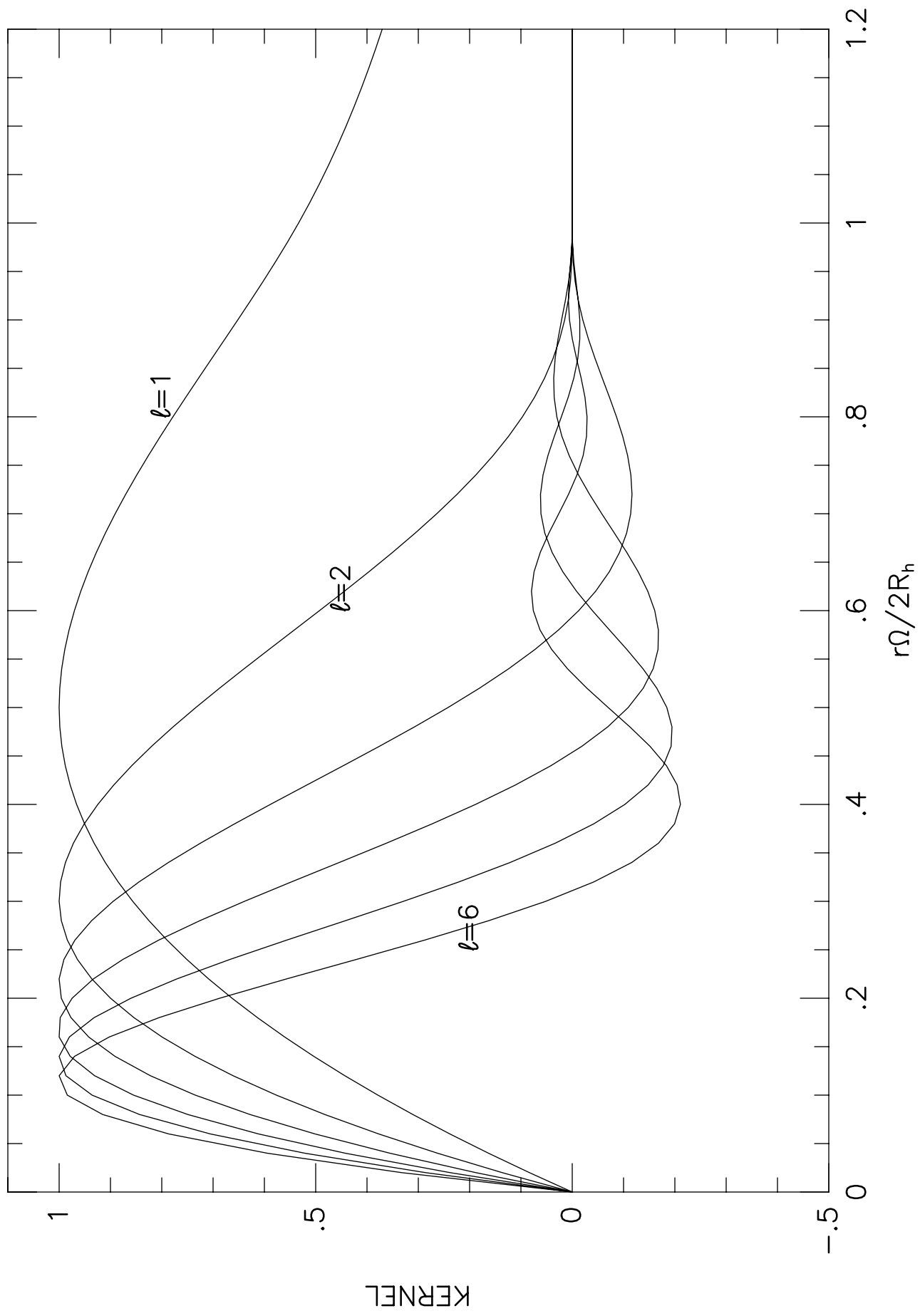


FIGURE 3b



This figure "fig1-4.png" is available in "png" format from:

<http://arxiv.org/ps/astro-ph/9402032v1>

This figure "fig2-4.png" is available in "png" format from:

<http://arxiv.org/ps/astro-ph/9402032v1>

FIGURE 4a

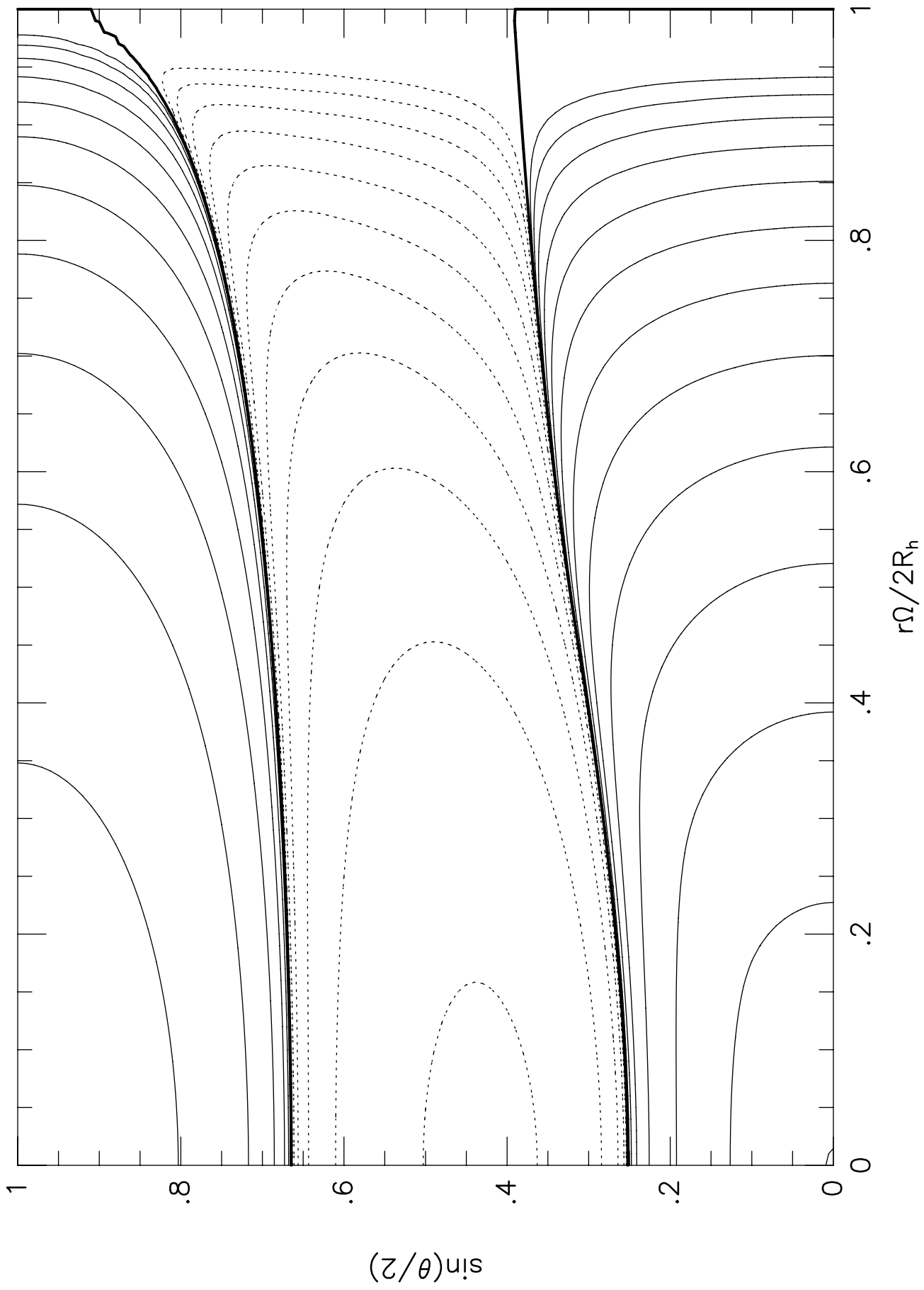
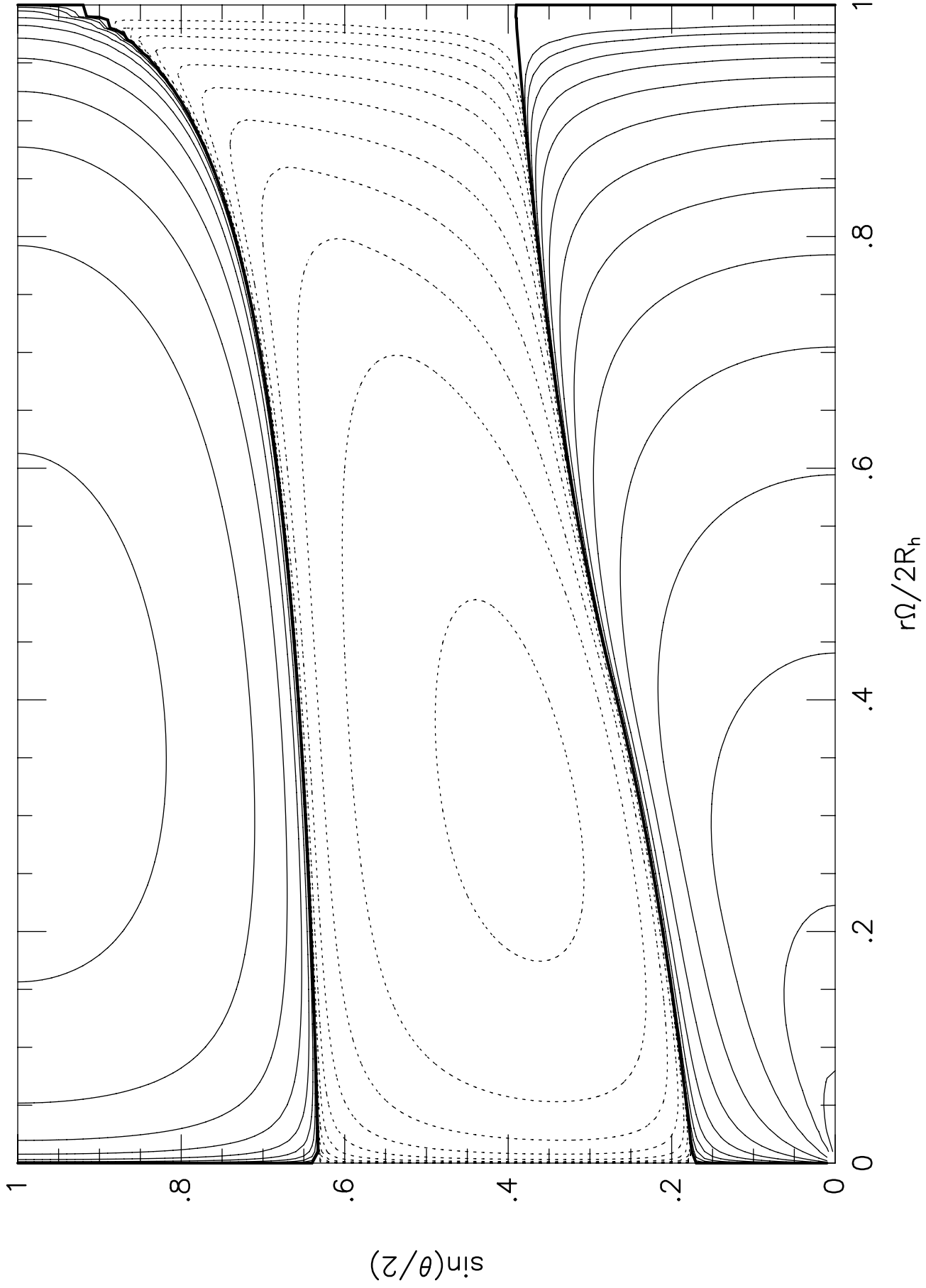


FIGURE 4b



This figure "fig1-5.png" is available in "png" format from:

<http://arxiv.org/ps/astro-ph/9402032v1>

FIGURE 5

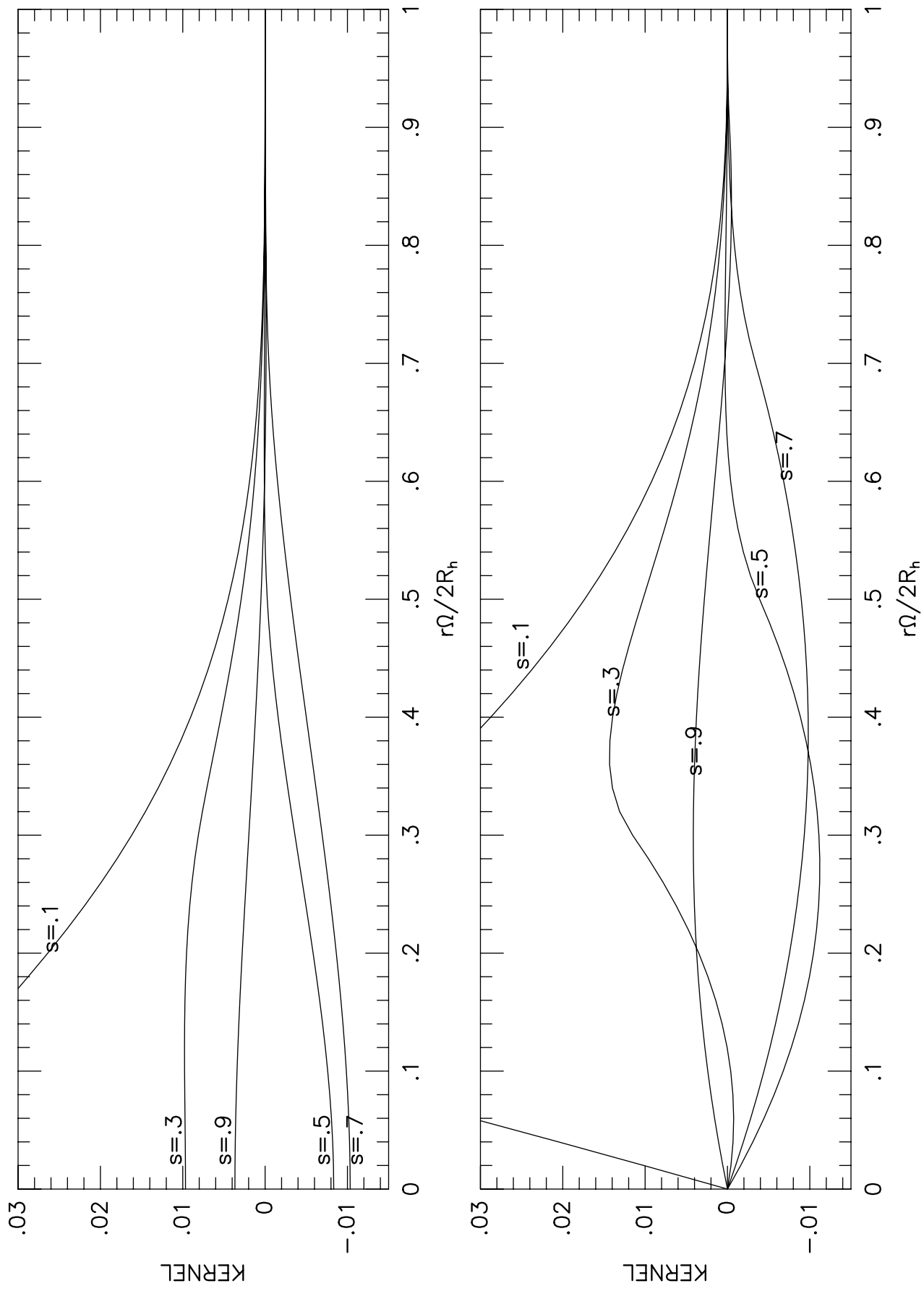


FIGURE 6

